CFD-BASED SIMULATION OF THE FLOW AROUND A SHIP IN OBLIQUE MOTION AT LOW SPEED

(DOI No: 10.3940/rina.ijme.2016.a4.374)

J Chen, **Z J Zou** and **M Chen**, Shanghai Jiao Tong University, China, and **H M Wang**, Zhejiang Ocean University, China

SUMMARY

Ships tend to maneuver in oblique motion at low speed in situations such as turning in a harbor, or during offloading, dynamic positioning and mooring processes. The maneuverability criteria proposed by IMO are valid for ships sailing with relatively high speeds and small drift angles, which are inadequate to predict ship maneuverability in low speed condition. Hydrodynamic performance of ships maneuvering at low speed is needed to know for safety issues. A CFD-based method is employed to predict the flow around an Esso Osaka bare hull model in oblique motion at low speed, where the drift angle varies from 0° to 180°. The URANS method with the SST k-ω model is used for simulating ship flows with drift angles 0°~30° and 150°~180°, and DES method for simulating ship flows with drift angles 40°~150°. Verification and validation studies are conducted for drift angles of 0° and 70°. The vortex structures at typical drift angles of 0°, 30°, 50°, 70°, 90° and 180° are analyzed. The effects of drift angle and ship speed are demonstrated.

1. INTRODUCTION

The operational demand of maneuvers in a harbor, in emergency situations to avoid collision, in offloading, dynamic positioning or mooring processes motivates the study of ship maneuverability at low speed. The IMO criteria emphasize ship maneuverability at service speed with relatively small drift angles. From the viewpoint of navigation safety, however, in-depth research is needed to understand the hydrodynamic performance of ships maneuvering in low speed condition with large drift angles.

Traditionally, the ship maneuvering problem is studied by model tests or by numerical methods based on potential theory. Oltmann and Sharma (1984) [1] conducted experimental research on a single-screw tanker and a twin-screw center-rudder container carrier, and proposed a maneuvering model based on the test results, taking account of the hull-propeller-rudder interaction in four quadrants. The main advantages of this model are its applicability to forward and backward motions. Tanaka and Kijima (1993, 1994) [2, 3] proposed a theoretical method on basis of vortex model by using the distribution of free vortices to represent the two-dimensional separated flow around the ship's section. The cross-flow drag of each section was obtained for ships undergoing oblique motion with large drift angles. This method was applied to the Wigley hull and a container ship hull. The calculated lateral forces and yaw moments agreed well with the measured results of oblique towing model tests. Yoshimura et al (2009) [4] developed a simple and unified mathematical model for ship maneuvering motion. They divided the hull force into a linear part and a nonlinear cross-flow drag part. The nonlinear part was estimated based on Oltmann and Sharma's cross-flow drag theory (1984) [1]. Oltmann and Sharma expressed the cross-flow drag coefficient by using the high-order polynomials, whereas Yoshimura et al. introduced correction factors by taking account of the effect of lateral velocity and yaw rate on the hull force. The difference of the hull force between ahead and astern conditions was considered. This model is also valid for the turning motion in which the forward speed is zero, and is believed to be able to well describe the maneuvering motions from ocean going to harbor maneuvering. Karasuno et al. (2003) [5] developed a component-type 4 degrees of freedom mathematical model to simulate slow speed maneuvering with a broad range of drift angles and yaw rates. The experimental method of PMM tests was adopted to determine the quasi-stationary hydrodynamic forces acting on a ship's hull. This maneuvering model was applied to the Esso Osaka for a 35° turning test and a 10°/10° zig-zag test. Beukelman and Journée (2001) [6] carried out tests with a ship-like wing model as well as tests with a seven-segments ship model to measure the lateral forces in deep and shallow water. The distribution of the cross-flow drag coefficient over the ship length was obtained from the segmented model tests. An empirical method was derived to estimate the distribution of the nonlinear lateral force component over the ship length. Hooft (1994, 1996) [7, 8] investigated the correlation factors based on Beukelman's segmented model tests (1988) [9], and found that the local cross-flow drag coefficient did not only depend on the drift angle but also on the turning rate. Both the linear part and the nonlinear part were determined by the ship's hull form parameters like the block coefficient, the draft and trim of the ship. Oh and Hasegawa (2012, 2013) [10, 11] summarized five mathematical models of hydrodynamic forces relating to low speed maneuver which were proposed by previous researchers based on model tests in wide range of the drift angles. Sway force and yaw moment were calculated for a tanker model using these five mathematical models and validated by comparing them with experiment results. Basic maneuvering simulations including turning test and zig-zag test were conducted for a single-propeller twin-rudder ship. The simulated

trajectories showed good agreement with those predicted by using these five mathematical models.

Nowadays, CFD (Computational Fluid Dynamic) method has been widely applied to deal with the maneuver problem. Xing et al. (2007) [12] investigated the flow around the KVLCC2 model at drift angles of 0°, 12°, 30°, and 60°, where the free surface effect was neglected. The RANS solver CFDShip-Iowa-V4 was employed. Flow details like limiting streamlines, vortical structures and associated instabilities were analyzed. Pinto-Heredero et al. (2010) [13] simulated flow around a Wigley hull at four different drift angles 10°, 30°, 45° and 60°, with the free surface effect being taken into account. The RANS method was used for steady ship flows, while the DES (detached eddy simulation) method was used to predict the unsteady flows. Fathi et al. (2010) [14] predicted the current loads on a LNG carrier with all appendages at model scale under flow angles between 0° and 180°. The mesh convergence studies were conducted. The comparison of force coefficients between experiments and computations showed that CFD can provide good qualitative predictions. Koop and Bereznitski (2011) [15] obtained the current load coefficients of a semi-submersible for all heading angles. An extensive verification study was carried out using ten different grids of different type for three different heading angles. Full scale force coefficients were calculated using five subsequently refined grids for these three different heading angles. On average the full-scale values were approximately 15%~20% lower than the model-scale results.

In this paper, a CFD-based method is adopted to predict the hydrodynamic characteristics of the Esso Osaka bare hull model in oblique motion at low speed with drift angles varying from 0° to 180°. The CFD software FLUENT is employed. RANS method with the SST *k-ω* model is adopted for drift angles 0°~30° and 150°~180°, and DES method is employed for drift angles 40°~150°. Verification and validation studies are conducted for the flows under drift angles 0° and 70°. The vortex structures of the flows at drift angles 0°, 30°, 50°, 70°, 90°, 180° are analyzed. The influence of drift angle on the lateral force and yaw moment is analyzed. The effect of ship speed in low speed region is shown.

2. MATHEMATICAL FORMULATIONS AND NUMERICAL SOLUTION

A ship moving obliquely at low speed in calm water is considered, as shown in Fig. 1. Two right-handed coordinate systems, $O-x_0y_0z_0$ and $o-xyz$, are adopted. The coordinate system $O-x_0y_0z_0$ is earth-fixed, with the $O-x_0y_0$ plane lying at the undisturbed free surface and z_0-axis pointing vertically downwards. The coordinate system $o-xyz$ is body-fixed, with the origin of the coordinate system located at the gravity center of the ship, the x-axis pointing towards the bow, the y-axis towards the starboard. U_0 is the ship speed, β is the drift angle. X_H is the longitudinal force acting on the ship, Y_H is the lateral force, N_H is the yaw moment.

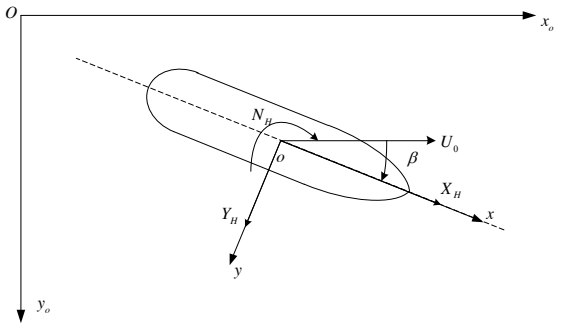

Figure. 1 Coordinate systems

2.1 GOVERNING EQUATIONS

The governing equations for the viscous flow around the ship are the following continuity equation and unsteady Reynolds Averaged Navier-Stokes (URANS) equations:

$$\begin{cases} \dfrac{\partial u_i}{\partial x_i} = 0 \\ \rho\dfrac{\partial u_i}{\partial t} + \rho u_j \dfrac{\partial u_i}{\partial x_j} = -\dfrac{\partial p}{\partial x_i} + \dfrac{\partial}{\partial x_j}\left(\mu\dfrac{\partial u_i}{\partial x_j} - \rho\overline{u_i'u_j'}\right) \end{cases} \quad (i, j = 1,2,3) \tag{1}$$

where x_i is the ith component of coordinate system, u_i and u_j are the mean velocity components, p is the mean pressure, ρ is the density of water, μ is the dynamic viscosity, $\rho\overline{u_i'u_j'}$ is the Reynolds stress.

2.1 (a) SST *k-ω* model

To close the governing equations, turbulence modeling is needed. Two typical turbulence models are most commonly used, namely the two equation *k-ε* model and *k-ω* model. The *k-ε* model is generally applicable only to the high Reynolds number flows with a homogenous turbulence structure, in which production and dissipation of turbulence are in balance. The *k-ε* model deteriorates when the turbulence structure is no longer close to local equilibrium. This modeling approach is considered to be unsatisfactory in steady ship flows. The *k-ω* model is proposed to account for the strong non-equilibrium effect which is likely to lead to separation. It is more accurate and reliable for flows under strong adverse pressure gradients. As shown in Fathi et al. (2010) [14], Koop and Bereznitski (2011) [15] and Wang (2009) [16], the shear-stress transport (SST) *k-ω* model gives more satisfactory results in modeling oblique ship motions.

The SST *k-ω* model was developed by Menter (1994) [17]. It effectively combines the robust and accurate formulation of the *k-ω* model in the near-wall region

with the free-stream independence of the *k*-ε model in the far field, and incorporates a damped cross-diffusion derivative term in the ω equation. It employs the automatic scalable wall functions, selecting the near wall treatment according to the y^+ value. Transport equations for the SST *k*-ω model can be expressed as follows:

$$\frac{\partial(\rho k)}{\partial t}+\frac{\partial(\rho k u_i)}{\partial x_i}=\frac{\partial}{\partial x_j}\left[\Gamma_k\frac{\partial k}{\partial x_j}\right]+\tilde{G}_k-Y_k+S_k \tag{2}$$

$$\frac{\partial(\rho \omega)}{\partial t}+\frac{\partial(\rho \omega u_i)}{\partial x_i}=\frac{\partial}{\partial x_j}\left[\Gamma_\omega\frac{\partial \omega}{\partial x_j}\right]+G_\omega-Y_\omega+D_\omega+S_\omega \tag{3}$$

where $\tilde{G}_k$ and G_ω represent the generation of turbulence kinetic energy, Y_k and Y_ω represent the dissipation of *k* and ω equations, respectively. Γ_k and Γ_ω represent the effective diffusivity. Other details of the SST *k*-ω model can be found in Menter (1994) [17].

2.1 (b) DES model

Jeans et al. (2009) [18] concluded that for slender axisymmetric bodies, flow asymmetry is not present (or very small) at drift angles up to 30°. Beyond this range, asymmetric flow grows, resulting in unsteady vortex shedding. Pinto-Heredero et al. (2010) [13] found that URANS method can capture the gross features of the unsteady separation and identify the important instabilities, but with deficiency in the amplitude of oscillation frequencies. Compared to URANS, DES predicts much broader frequency ranges in terms of unsteady flows. It can resolve more flow physics and provide a much better analysis of the turbulent structures. Since unsteady flow separation would be influential when the ship moves at larger drift angles, DES model is adopted in the present study to simulate these unsteady flows.

The DES model usually refers to LES/RANS coupling modeling approach. It is based on the assumption that RANS models are capable of modeling attached boundary layer flows, so that the LES model is only required in the outside regions of separated flow. As most ship flows contain large areas of attached boundary layer flow, the computational cost is reduced by using RANS method in these regions, overcoming the disadvantage of LES model with high computational cost.

This combination is achieved through the modification of the length scale in the turbulence model. The length scale $\tilde{l}$ in DES model is related to the grid spacing away from the wall. It is defined as $\tilde{l}=\min(l_{RANS}, C_{DES}\Delta_{\max})$, where $\Delta_{\max}$ is the largest dimension of the grid. Within DES model, the switch between RANS and LES is based on the criterion:

$$\begin{aligned} &C_{DES}\Delta_{\max} > L_t, \quad \text{RANS} \\ &C_{DES}\Delta_{\max} \le L_t, \quad \text{LES} \end{aligned} \tag{4}$$

where the grid length scale L_t in the SST *k*-ω model is defined as $L_t=\sqrt{k}/(\beta^*\omega)$, $\beta^*=0.09$. $C_{DES}=0.65$ defines the transition point between the DES and RANS modes.

Since many efforts are devoted to the mesh generation, it is crucial to determine the gird size required by DES model. The Separating Shear Layer (SSL) is introduced. It refers to the shear layer that starts at the point of separation from the body and moves into a free shear flow. In the case of locally unstable flows, the maximal spacing should be sufficiently small to allow resolution of the initial flow instability of the SSL. The main quantity of relevance is the ratio of the largest dimension of the grid $\Delta_{\max}$ to the grid length scale L_t:

$$R_L=\Delta_{\max}/L_t, \quad (R_L \le 0.2\sim 0.1) \tag{5}$$

where 0.2 is an extreme lower limit of resolution and 0.1 is the desirable lower limit.

2.2 BOUNDARY CONDITIONS

Figure 2 shows the computational domain and the boundary conditions. Figure 2(a) demonstrates the relative position of the ship in the computational domain, and L_{pp} is the ship length. Different drift angle is achieved by rotating the ship hull with a drift angle about its center of gravity. The height of the computational domain extends from the undisturbed free surface to a depth of $1.2L_{pp}$. By a series of numerical experiment, it has been proven that the size of the computational domain is large enough to attain the domain-independent solutions. As shown in Figure. 2(b), the velocity-inlet condition is imposed on the inflow boundary. In the outflow boundary plane, a pressure-outlet condition is applied. A no-slip condition is imposed on the hull surface. The effect of free surface elevation is neglected due to the low ship speed; the topside boundary, i.e., the undisturbed free surface, is specified as "symmetry" boundary to simulate the double-model flow. On the bottom boundary, the velocity-inlet condition is imposed.

The velocity and turbulent quantities are specified at the inflow boundary. The initial value of turbulent energy, *k*, is computed as $k=1.5(UI)^2$, where *U* is the mean flow velocity; *I* is the turbulence intensity, $I=0.05\sim 0.2$ in most ship flows and $I=0.05$ is chosen in the present study. The specific turbulent dissipation rate, ω, is computed using the formulas: $\omega=C_\mu^{-\frac{1}{4}}\sqrt{k}/l$, where C_μ is a turbulence model constant which usually has a value of 0.09; l is the turbulent length scale, $l=0.1L_{pp}$ for most ship flows.

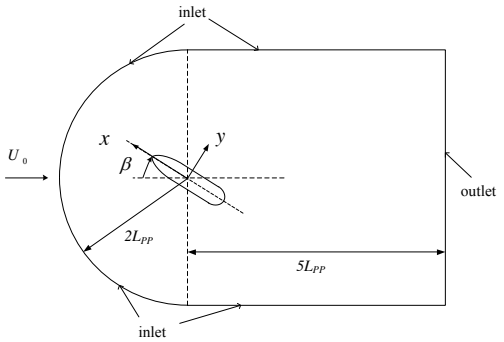

(a) Top view of the computational domain

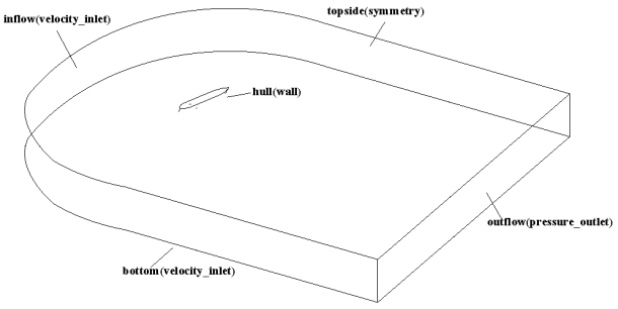

(b) Boundary conditions

Figure 2. Computation domain and boundary conditions

2.3 NUMERICAL SOLUTION

The numerical simulations are performed by using the CFD software FLUENT. The pressure equation is discretized by second order scheme, while the momentum equations and turbulence equations are discretized by second order upstream scheme to guarantee the calculation accuracy. The SIMPLEC algorithm is applied to solve the velocity-pressure coupling problem. Structured meshes are generated using the meshing program POINTWISE. The benefits of using a structured mesh rather than an unstructured mesh are that it requires less memory and is easier to align with the flow direction, which minimizes the numerical diffusion. The height of the first cell on the hull surface is chosen to ensure $y^+<5$.

3. CASE FOR STUDY

The tanker Esso Osaka is selected for the computation, which is considered as a benchmark case in maneuvering condition. Figure 3 shows the hull form geometry. The main particulars of the hull form are given in Table 1.

Figure 3. Hull form geometry of Esso Osaka

Table 1 Main particulars of Esso Osaka

Particulars	Full scale	Model scale (1:43.47)
Length L_{pp} (m)	325	7.475
Beam B (m)	53	1.219
Draft T (m)	22.05	0.501
Block coefficient C_B	0.831	0.831
Displacement ∇ (m^3)	319455	3.889

The computational domain is divided into multiple blocks, as shown in Figure 4. The blocks surrounding the ship remain the same for all drift angles, while the remaining blocks are deformed to suit the boundary conditions. In this way, grids for various drift angles can be generated efficiently. The grid on the topside of the computational domain at β=110° is shown in Figure 4(a), and the grid on the hull surface is shown in Figure 4(b).

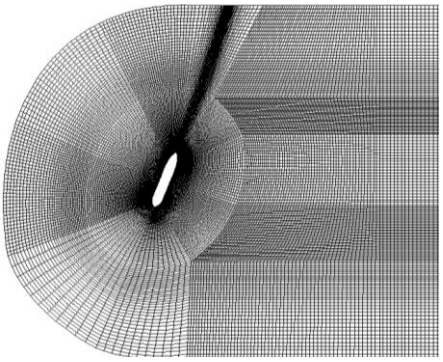

(a) Topside at β=110°

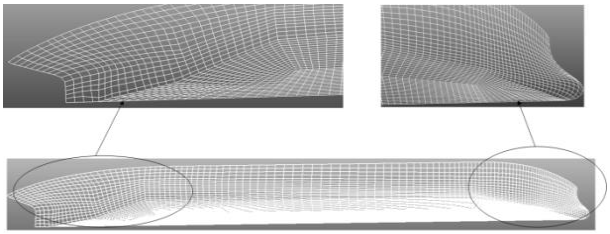

(b) Hull surface

Figure 4 Grid topology of the computational domain

The effect of drift angle is investigated by simulating the flow under different drift angles at a constant ship speed. To study the effect of the ship speed, computations are performed under several low speed conditions at β=90°. A summary of the computation cases are given in Table 2. The calculated longitudinal force, lateral force and yaw moment are presented in non-dimensional forms as:

$$X_H' = \frac{X_H}{\frac{1}{2}\rho L_{pp} T U_0^2}, \quad Y_H' = \frac{Y_H}{\frac{1}{2}\rho L_{pp} T U_0^2}, \quad N_H' = \frac{N_H}{\frac{1}{2}\rho L_{pp}^2 T U_0^2}$$

Table 2 Computation cases

Fr	β (°)	Turbulence model
0.0622	0, 2.5, 5, 7.5, 10, 15, 20, 30, 150, 160, 170, 175, 180	SST *k-ω* (steady)
0.0622	50, 60, 70, 80, 85, 90, 95, 100, 110, 120, 130, 140	DES (transient)
0.0611, 0.0584, 0.0467, 0.0351, 0.0234, 0.0117	60	

4. VERIFICATION AND VALIDATION

For the Esso Osaka ship model, Yumuro [19] conducted extensive experimental research including towing tank tests and circular motion tests, in which the drift angle varied between 0° and 180° in low speed condition. Simonsen and Stern [20-22] conducted CFD study and experimental research with small drift angles.

The methodology and procedures of verification and validation (V&V) follow Stern et al. [23]. The V&V are performed at β=0° and *Fr*=0.062 to validate the results in case of zero drift angle. The V&V procedure for unsteady flows are performed at β=70° and *Fr*=0.062. Unsteady simulation for flows at large drift angles using DES model is validated according to this procedure.

4.1 V&V OF STEADY FLOW AT β=0° AND *Fr*=0.062

Three systematically varied girds are designed with a uniform grid refinement ratio $r_G=\sqrt{2}$. The solution is stopped when the residuals reach a level of 10^{-5} or lower, which means that the iterative convergence is achieved. The results of grid verification study are given in Table 3, where the total longitudinal force X_H' is a sum of the pressure force component X_P' and the frictional component X_F'.

Table 3 Results of grid verification study (β=0°, *Fr*=0.062)

	Grid numbers	X_P'	X_F'	X_H'
Grid1	3390090	0.00493	0.01304	0.01797
Grid2	1086920	0.00491	0.01242	0.01733
Grid3	395488	0.00219	0.01150	0.01369

As shown in Table 3, the differences of X_H' between Grid1 and Grid2 is $\varepsilon_{G12}=0.064\%$, and between Grid2 and Grid3 is $\varepsilon_{G23}=0.364\%$. It gives the convergence ratio $R_G=\varepsilon_{G12}/\varepsilon_{G23}=0.175$. Since $0<R_G<1$, grid convergence is achieved. The estimated order of accuracy is $p_G=\ln(\frac{\varepsilon_{G23}}{\varepsilon_{G12}})/\ln(r_G)=5.017.$ Using the theoretical order of accuracy P_{GEST}=2, the correction factor is calculated as $C_G=(r_G^{P_G}-1)/(r_G^{P_{GEST}}-1)=4.691.$ When C_G is sufficiently larger than 1, the solution is away from the asymptotic range, and the uncorrected grid uncertainty is $U_G=\left(2\left|1-C_G\right|+1\right)\left|\delta^*_{RE_{G1}}\right|=0.00114$ =6.3%Grid1, where the one-term estimate for the error is $\delta^*_{RE_{G1}}=\varepsilon_{G_{12}}/(r_G^{P_G}-1)=-0.00013.$ Simonsen and Stern[20] provided the experimental value $\mathrm{EXP}=0.0183$ and its uncertainty $U_D=1.64\%$. The comparison error *E*=EXP $-X_H$'. The validation uncertainty is $U_V=\sqrt{U_D^2+U_G^2}.$ The V&V of X_H' with the finest grid Grid1 are summarized in Table 4. As it can be seen from this table, the comparison error E (1.96) is smaller than the validation uncertainty U_V (10.9), which means that X_H' is validated on a 10.9% level.

4.2 V&V OF UNSTEADY FLOW AT β=70° AND *Fr*=0.062

4.2 (a) Grid verification study

A grid verification study is carried out; three sets of grids are designed with a grid refinement ratio $r_G=\sqrt{2}$. Table 5 summarizes the grid uncertainties for the three sets of grids. As it can be seen from this table, N_H' tends to converge, while X_H' and Y_H' require finer grids to achieve convergence.

4.2 (b) Sub-iteration error study

The errors under different numbers of sub-iteration for a certain time step length are assessed by comparing the results obtained using the numbers of sub-iteration *sub_t*=10, 7 and 5, with the finest grid (Grid1). All these calculations are carried out with the same time step length Δt=0.005s. The results are shown in Table 6. As it can be seen from this table, the relative differences in the yaw moment coefficient N_H' at *sub_t*=7 and 5 with respect to *sub_t*=10 are 0.221% and 0.503%, respectively. Hence the sub-iteration error is negligible, and *sub_t*=5 is chosen for computation efficiency in the subsequent simulation.

Table 4 Verification and validation of X_H' (β=70°, Fr=0.062)

R_G	P_G	U_G (%Grid1)	EXP	E % EXP	U_V % EXP
0.175	5.017	6.3	0.01833	1.96	10.9

Table 5 Grid verification study (β=70°, Fr=0.062)

	Grid1	Grid2	Grid3	R_G	P_G	U_G (%Grid1)
X_H'	0.0391	0.0443	0.0373	-	-	-
Y_H'	0.6722	0.6412	0.6608	-	-	-
N_H'	0.0456	0.0468	0.0485	0.705	1.005	0.987

Table 6 Differences under different numbers of sub-iteration (β=70°, Fr=0.062)

sub_t	Y_H'	Difference of Y_H' (% *sub_t*=10)	N_H'	Difference of N_H' (% *sub_t*=10)
10	0.6743	-	0.04968	-
7	0.6795	0.78	0.04957	0.221
5	0.6812	1.03	0.04943	0.503

Table 7 Time-step verification results (β=70°, Fr=0.062)

	Δt_1	Δt_2	Δt_3	R_G	P_G	U_G (% Δt_3)
X_H'	0.0391	0.0443	0.0373	0.478	-	-
Y_H'	0.6333	0.6407	0.6743	0.22	4.367	1.885
N_H'	0.0462	0.0473	0.0496	-0.28	2.129	2.408

Table 8 Validation results (β=70°, Fr=0.062)

	CFD	EXP	E (%EXP)	U_V (%Δt_3)
Y_H'	0.6743	0.78595	14.206	1.29
N_H'	0.0496	0.04881	1.602	2.77

4.2 (c) Time step verification study

The time step length Δt determines the quality of the resolution of the turbulent structures. A typical shedding frequency f for the largest turbulent structures can be estimated based on the Strouhal number $St = fL_{pp}/U_0$. The universal St number lies in the range of 0.07~0.09 [12]. This results in a time-step length Δt=1/f varying between 0.005s and 0.01s. Three time-step lengths, Δt_1=0.01s, Δt_2=0.00707s and Δt_3=0.005s, are evaluated. The time-step verification results are shown in Table 7. As it can be seen from this table, monotonic convergence with uncertainties 1.885% (Δt_3) and 2.408% (Δt_3) is achieved for Y_H' and N_H', respectively, while oscillatory divergence is achieved for X_H'. Therefore, a time step length of 0.005s is used in the subsequent simulations.

4.2 (d) Validation study

Validations for X_H' cannot be conducted due to the lack of experimental data. Yumuro[19] provided the measured values of the lateral force and yaw moment, but did not give the uncertainty estimates of these values. The experimental uncertainty U_D=2.5% is used in the present study based on Xing et al.[12]. Validations for Y_H' and N_H' are shown in Table 8. It can be seen that N_H' is validated since the comparison error E (1.602) is smaller than the validation uncertainty U_V (2.77). On the other hand, Y_H' is not validated. Thus finer grids are needed for Y_H'.

5. NUMERICAL RESULTS

5.1 GLOBAL FORCES

Figure 5 shows the comparison of the predicted lateral force and yaw moment with experimental data at different drift angles and Fr=0.0622. Good agreement is achieved in case of small drift angles. The maximum deviation of the predicted Y_H' is 19.82% at β=30°. The maximum error of N_H' is 15.6% at β=130°.

In order to analyze the effect of ship speed, calculations are performed at β=60° and different Fr numbers, as given in Table 2. The results of X_H', Y_H' and N_H' are shown in Figure 6. It can be seen that the values of Y_H' decrease as Fr increases. The maximum value reaches

27.21% at the lowest Fr=0.0117. N_H' decreases slightly with Fr, which shows the limited influence of Fr on the force distribution along the ship hull. X_H' remains nearly constant as Fr increases.

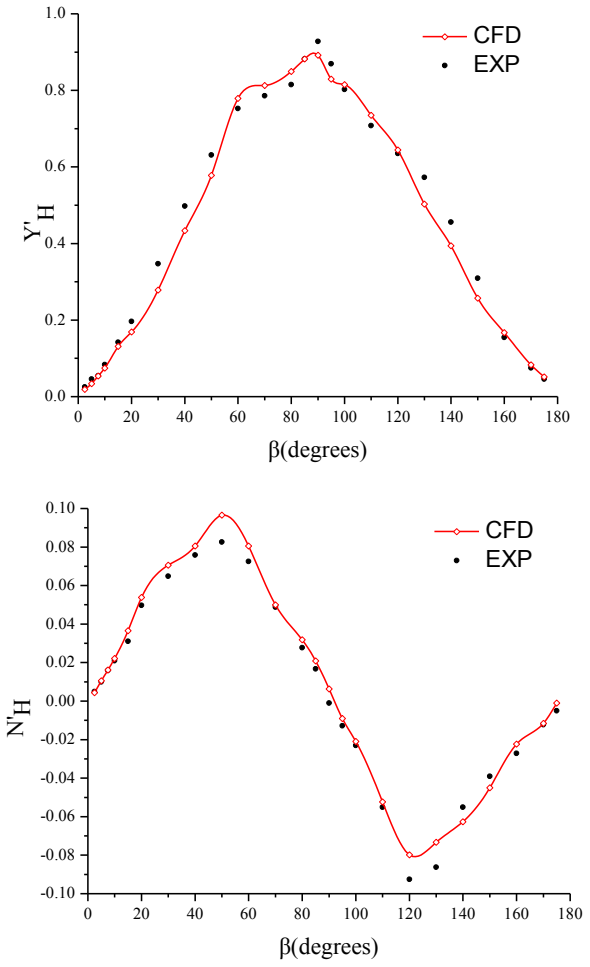

Figure 5. Comparison between CFD and EXP of Y_H' and N_H' versus drift angles, Fr=0.0622

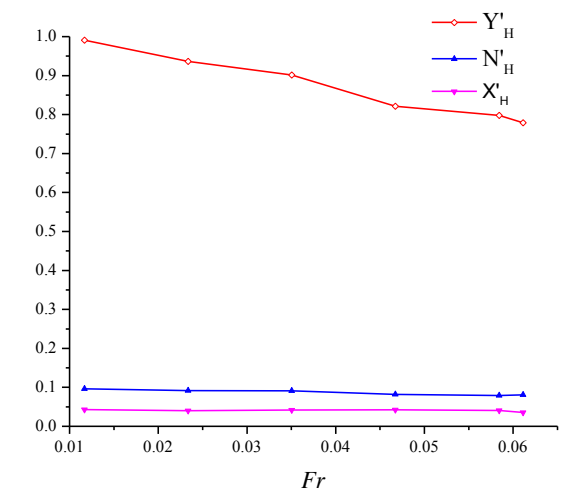

Figure 6. X_H', Y_H' and N_H' changing with Fr at β=60°

5.2 FLOW TOPOLOGY

The Q-criterion is a scalar used to visualize turbulent fields. It is sometimes preferred over the contours of vorticity components or the pressure field when large pressure gradients are present in the local low-pressure areas of the flow. When the Q-criterion is positive, it represents the locations in the flow where the rotation dominates the strain and shear.

The Q-criterion is defined by [24]

$$Q = \frac{1}{2}(\|\Omega_{ij}\|^2 - \|S_{ij}\|^2) \tag{6}$$

where Ω_{ij} is the vorticity, which is defined by

$$\Omega_{ij} = \frac{1}{2}\left(\frac{\partial u_i}{\partial u_j} - \frac{\partial u_j}{\partial u_i}\right) \tag{7}$$

S_{ij} is the strain rate which relates shear stress to the viscosity, and is defined by the second invariant of the rate-of-deformation tensor D_{ij}:

$$S_{ij} = \sqrt{\frac{1}{2}\bar{\bar{D}}_{ij} : \bar{\bar{D}}_{ij}}, \quad \bar{\bar{D}}_{ij} = \left(\frac{\partial u_j}{\partial x_i} + \frac{\partial u_i}{\partial x_j}\right) \tag{8}$$

Q contours on the transverse planes at several axial locations are introduced to describe the vortical structures. Q contours of flows at β=0° (forward motion) and β=180° (backward motion) are shown in Figure 7(a) and Figure 7(b), respectively. As shown in Figure 7(a), the flow is quite symmetric with small vortices in the stern region. In Figure 7(b), however, larger vortices become obvious in the bow region, which may have a significant influence on the longitudinal force, and the pressure component may reach the same order of magnitude of the frictional component.

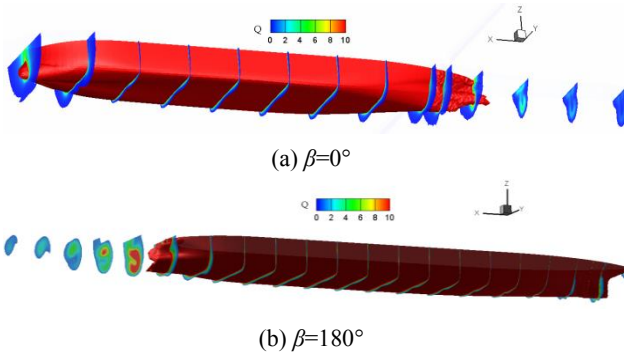

(a) β=0°

(b) β=180°

Figure 7. Vortical structures at β=0° and β=180°, Fr=0.0622

The instantaneous Q contours on the transverse planes at several axial locations with iso-surface Q=30 at β=30°, 50°, 70° and 90° are shown in Figure 8. Figure 8(a) shows the Q contours of flows at β=30°. Relatively small vortices are observed at the bow, stern and the bottom regions of the hull.

The Q contours of flows at β=50° are shown in Figure 8(b). Stronger vortices are generated at almost the same regions in comparison to that at β=30°. The Q contours of flows at β=70° are shown in Figure 8(c). Complex and unsteady vortices on the leeward side of the hull are generated. Ship flow separates at the bow, stern and the bottom regions of the hull. A large recirculation region is formed in the leeward side of the hull, because of the interaction between the flow coming from the fore end and that below the keel. The Q contours of flows at β=90° are shown in Figure 8(d). Large-scale turbulent structures are generated in the bottom region of the hull. The interactions between the flow from the bottom region and those from the bow and stern areas result in large recirculation region on the bottom of the hull. It can be observed that the vortices generated around the bow and the stern on the leeward side of the hull become stronger at β=50°, and are less obvious at β=90°. Vortical structures produced at the bottom of the hull have the largest scale at β=90°.

6. CONCLUSIONS

CFD-based methods are employed to simulate the viscous flow around the Esso Osaka bare hull model in oblique motion at low speed, where the drift angle varies from 0° to 180°. RANS method is adopted to simulate the steady ship flows at drift angles 0°~30° and 150°~180°, while DES method is employed to simulate the unsteady ship flows at drift angles 40°~150°. The longitudinal force X_H, lateral force Y_H and yaw moment N_H acting on the hull in oblique motion with various drift angles are predicted. The verification and validation studies are performed for drift angle β=0° and β=70°. From this numerical study, the following conclusions can be drawn:

(1) X_H' is validated on a 10.9% level at β=0° and Fr=0.062. In case of β=70°, N_H' is validated with the validation uncertainty U_V =2.77; however, finer grids are needed for the validation of Y_H'.

(2) URANS method with the SST k-ω model can give satisfactory prediction results of hydrodynamic forces for drift angles 0°~20° and 160°~180°.

(3) DES method for the unsteady flows at drift angles 30°~150° can give the acceptable numerical results for engineering application. The maximum deviation of the predicted Y_H' from the experimental value is 19.82% at β=30°. The maximum error of N_H' is 15.6% at β=130°.

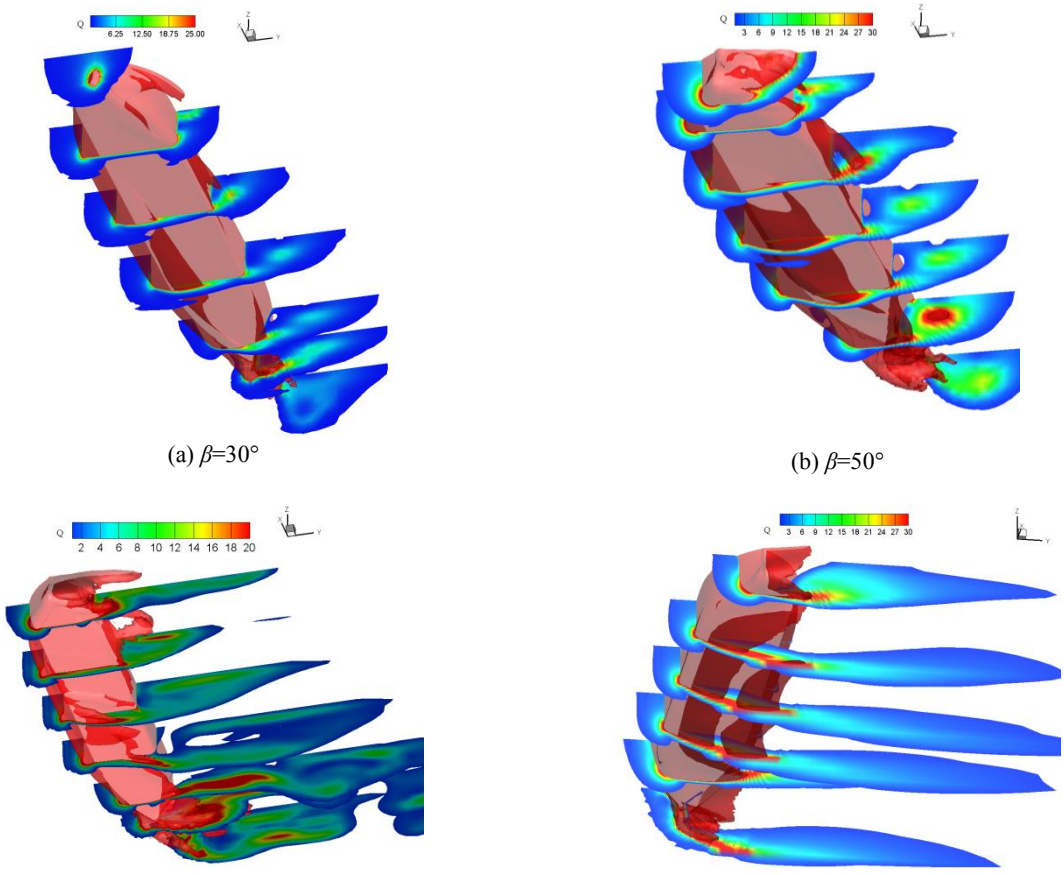

(a) β=30° (b) β=50°

(c) β=70° (d) β=90°

Figure 8. Vortical structures at various drift angles, Fr=0.0622

(4) The global forces decrease slightly with the increasing ship speed in low speed region. The ship speed has only remarkable influence on the lateral force.

(5) Stronger vortices are observed in the backward motion compared to that in the forward motion, resulting in larger longitudinal forces.

(6) Large scale turbulent structures are formed in the bow and stern regions in the leeward side of the hull in case of β=50°. The strongest vortices under the bottom area are observed in cross flow at β=90°.

7. ACKNOWLEDGEMENTS

This work is financially supported by the National Natural Science Foundation of China (Grant No. 51309152) and the Natural Science Foundation of Zhejiang Province, China (Grant No. LY16E090004)

8. REFERENCES

1. OLTMANN, P. and SHARMA, S.D. Simulation of Combined Engine and Rudder Manoeuvres Using an Improved Model of Hull-propeller-rudder Interactions, *Proc. of 15th Symposium on Naval Hydrodynamics*, *pp.83-108,* 1984.
2. TANAKA, S. and KIJIMA, K. On the Distribution of Cross Flow Drag over the Length of a Ship Moving Transversely. *J Soc Naval Arch Japan*, *Vol.174. pp 357-363*, 1993.
3. TANAKA, S. and KIJIMA, K. Calculation of Cross Flow Forces Acting on a Ship at Larger Drift Angles. *J Soc Naval Arch Japan, Vol.176. pp 251-258*, 1994
4. YOSHIMURA, Y. NAKAO, I. and ISHIBASHI, A. Unified Mathematical Model for Ocean and Harbor Manoeuvring, *Proc. of MARSIM 2009*, *pp.116-124*, 2009.
5. KARASUNO, K., OKANO, S. and MIYOSHI, J. et al. Predictions of Ship's Hull Hydrodynamic Forces and Maneuvering Motions At Slow Speed Based on a Component-type Mathematical Model, *Proc. of MARSIM'03*, *pp. RC-4-1~11*, 2003.
6. BEUKELMAN, W. and JOURNÉE, J.M.J. Hydrodynamic Transverse Loads on Ships in Deep and Shallow Waters, *Prof. of 22nd International Conference on Hydrodynamics and Aerodynamics in Marine Engineering*, 2001.
7. HOOFT, J.P. The Cross-flow Drag on a Manoeuvring Ship, *Ocean Engineering*, *21(3), pp.329-342*, 1994.
8. HOOFT, J.P. and QUADVLIEG, F.H.H.A. Non-linear Hydrodynamic Hull Forces Derived from Segmented Model Tests, *Proc of MARSIM'96*, *pp.399-409*, 1996.
9. BEUKELMAN, W. Longitudinal Distribution of Drift Forces for a Ship Model. *Technical University of Delft, Department of Hydronautica*, *Report No. 810*, 1988.
10. OH, K.G. and HASEGAWA, K. Ship Manoeuvring Hydrodynamic Forces and Moment in Low Speed, *Proc. of AMEC 2012*, *Paper No.SNOM-09*, 2012.
11. OH, K.G. and HASEGAWA, K. Low Speed Ship Manoeuvrability: Mathematical Model and its Simulation, *Proc. of OMAE2013*, *OMAE2013-11489*, 2013.
12. XING, T., SHAO, J. and STERN, F. BKW-RS-DES of Unsteady Vortical Flow for KVLCC2 at Large Drift Angles. *Proc. of 9th International Conference on Numerical Ship Hydrodynamics*, 2007.
13. PINTO-HEREDERO, A., XING, T. and STERN, F. URANS and DES Analysis for a Wigley Hull at Extreme Drift Angles. *J Mar Sci Technol*, *15*, *pp.295-315*, 2010.
14. FATHI, F. KLAIJ, C. and KOOP, A. Predicting Loads on a LNG Carrier with CFD. *Proc. of OMAE2010*, 2010
15. KOOP, A. and BEREZNITSKI, A. Model-scale and Full-scale CFD Calculations for Current Loads on Semi-submersible. *Proc. of OMAE2011*, 2011.
16. WANG, H.M. Numerical Study on the Viscous Flow and Hydrodynamic Forces on a Manoeuvring Ship in Restricted Waters (in Chinese). *Dissertation at Shanghai Jiao Tong University*, 2009.
17. MENTER, F.R. Two-equation Eddy-viscosity Turbulence Models for Engineering Applications, *AIAA Journal*, *32(8)*, *pp.1598-1605*, 1994.
18. JEANS, T.L., WATT, G.D., GERBER, A.G., et al. High-resolution Reynolds-averaged Navier Stokes Flow Predictions over Axisymmetric Bodies with Tapered Tails. *AIAA Journal*, *47(1)*, *pp.19-32*, 2009.
19. YUMURO, A. Some Experiments on Maneuvering Hydrodynamic Forces in Low Speed Condition, *Journal of the Kansai Society of Naval Architects*, *Vol. 209*, *pp. 91-101*, 1988.
20. SIMONSEN, C.D. and STERN, F. Verification and Validation of RANS Maneuvering Simulation of Esso Osaka: Effects of Drift and Rudder Angle Forces and Moments. *Computers & Fluids*, *32(10)*, *pp.1325-1356*, 2003.
21. SIMONSEN, C.D. and STERN, F. Flow Pattern around an Appended Tanker Hull Form in Simple Maneuvering Conditions, *Computers & Fluids, 34(2), pp169-198*, 2005.
22. SIMONSEN, C.D. and STERN, F. RANS Maneuvering Simulation of Esso Osaka with

Rudder and a Body-force Propeller. *Journal of Ship Research*, *49(2)*, *pp*. *98-120*, 2005.

23. STERN, F. WILSON, R.V. COLEMAN, H. and PATERSON, E. Verification and Validation of CFD Simulations. *Iowa Institute of Hydraulic Research*, *IIHR Report*. *No.407*, *The University of Iowa*, 1999.
24. HUNT, J.C.R. WRAY, A.A. and MOIN, P. Eddies, Stream, and Convergence Zones in Turbulent Flows. *Center for Turbulence Research Report CTR-S88*, *pp.193-208*, 1988.

